KECK Geology Consortium
Learning Science Through Research
Published by the Keck Geology Consortium
Short Contributions
Keck Geology Consortium
Volume 36
May 2024
doi: 10.18277/AKRSG.2024.36.03

COMPUTER MODELING OF NORMAL FAULT-RELATED DAMAGE ZONES: IMPLICATIONS FOR ESTIMATING GEOTHERMAL ENERGY POTENTIAL

AUDREY JENNINGS, Trinity University
Project Advisor: Benjamin Surpless

INTRODUCTION

In the 21st century, many nations have sought to diversify their energy resources to promote energy security and slow climate change impacts (e.g., Boden, 2017). New renewable energy resources, such as geothermal energy, can help achieve this. To be productive at the utility-scale, geothermal energy systems require high subsurface heat flow and connected fluid pathways. Fault damage zones are conducive to geothermal energy production due to the high stresses and strain created by faulting, which can increase subsurface permeability due to intense fracturing (e.g., Micale et al., 2014; Faulds and Hinz, 2015; Shervais et al., 2024). Thus, further investigating damage zone formation in normal fault zones is a crucial step in expanding geothermal energy production in the United States.

However, field-based geothermal exploration can be prohibitively expensive, making lower-cost exploration options like 3D computer modeling appealing (e.g., Micale et al., 2014; Shervais et al., 2024). Therefore, this study utilized 3D modeling to assess the influence of different geologic variables (including fault displacement, fault propagation, and pore fluid pressure) on damage zone development in a simple normal fault system. Through this work, I aim to answer a range of research questions, including:

1. How do stress, strain, and fracturing evolve as faults propagate, and how do different fault propagation models impact the evolution of deformation?

2. What effects do fault-related stress and strain fields have on fracturing orientations and intensities within the rock volume?

3. How does the distribution of fault-related fracturing vary with depth and accumulated displacement?

4. Can we use 3D modeling results to aid in the identification of locations with especially high permeability and thus geothermal potential?

BACKGROUND

Geothermal energy production

Production sites for geothermal energy development must provide both elevated heat flows and high permeabilities. Traditional strategies for permeability identification, such as drilling into the subsurface to look for the presence of heated, mobile fluids (e.g., Boden, 2017), can be effective but typically require upfront financial investment that may not be recouped if they fail to locate the desired setting (e.g., Micale et al., 2014).

Further investigation of damage zones can be helpful for geothermal system locations because zones tend to form in predictable patterns, with the greatest intensity of fracture and shear-related deformation near the fault center. (e.g., Berg and Skar, 2005; Savage and Brodsky, 2011; Choi et al., 2016). Damage zones also often form asymmetrically, with the width and intensity of deformed regions differing between the hanging wall (HW) and footwall (FW) (e.g., Berg and Skar, 2005; Choi et al., 2016; Liao et al., 2020). Furthermore, faults propagate laterally and accumulate displacement over their life, causing damage zones to potentially vary based on stage of fault growth.

However, patterns of fault propagation are not entirely understood. The fault propagation (FP) model posits that a fault lengthens horizontally as it accumulates vertical displacement, such that the fault is growing horizontally and vertically at the same rates (e.g., Cowie et al., 2000; Kim and Sanderson, 2005; Rotevatn et al., 2019). In contrast, the constant length (CL) model describes an initial rapid accumulation of horizontal length and then an accumulation of dip-slip displacement (e.g., Cowie, 1998; Nicol, 2005; Rotevatn et al., 2019). However, neither conceptual model has emerged as a more accepted model of fault growth (Rotevatn et al., 2019). Because fault propagation and associated displacement accumulation are the most significant sources of stress, strain, and fracturing within normal fault systems, better understanding the implications of both models for the evolution of stress, strain, and fracture development is critical for evaluating damage zones associated with faults at locations with high geothermal potential.

METHODS

Model construction

To investigate damage zone development in normal fault zones, I utilized the Fault Response Modeling (FRM) module of Move 2022 (by Petex). This module calculates 72 distinct geologic variables based on user-designed 3D fault scenarios. It also utilizes boundary element modeling (BEM), calculating specified variables only at defined observation points across the model in order to reduce computing power but maintain accuracy (Petex, 2020). Such calculations are based on the movement and flexure of blocks of material relative to the fault plane. I constructed three different sets of fault models, calculating the resulting values for variables of interest ((maximum Coulomb shear stress, E1 (strain value in the orientation of maximum strain), and strain dilation (increase in volume related to rock deformation)) at the meter scale across 3 different depths (0.5 km, 2 km, and 3 km). Using the FRM module I also generated predictions of fracture orientation and intensity across each model. Data is shown via heatmaps for each variable, with warmer colors indicating higher variable values and larger dots representing more intense fracturing. In addition to these heatmaps, I also exported the raw numerical data for each variable and graphed it across defined cross-fault profiles in order to visualize spatial changes in stress and strain.

Each model consists of a single, 5 km-long fault segment dipping at 70 degrees from the horizontal (Fig. 1). I also set every observation surface to mimic the lithological properties of the Navajo sandstone, including a Young's Modulus of 30,000 MPa, a Poisson's Ratio of 0.25, and a density value of 2,495 kg/m^3 (Schultz, 2010). The Navajo sandstone is present throughout much of the Basin and Range province (e.g., Fossen et al., 2011), a promising region for geothermal development due to the intense faulting and high heat flow found throughout (e.g., Faulds and Hinz, 2015). By defining the properties of our observation surfaces to be like the Navajo Sandstone, results can be better applied to real world geothermal potential. I also defined pore fluid pressures of 5.2 MPa for the 0.5 km-depth surface, 20.6 MPa for the 2 km-depth surface, and 36.0 MPa for the 3 km-depth surface of every model, as well as a model with a pore fluid pressure value of 0 MPa for each observation surface depth, serving as a control model to compare stress, strain, and fracturing results across fluid conditions.

To model the potential impacts of the fault propagation (FP) model on damage zone development, I constructed three different normal fault segment models which mimic a simultaneous increase in vertical displacement and lateral increase in fault length. To simulate fault development according to the constant length (CL) propagation model, I kept the fault segment at 6 km of length across all three models and gradually increased the vertical displacement in

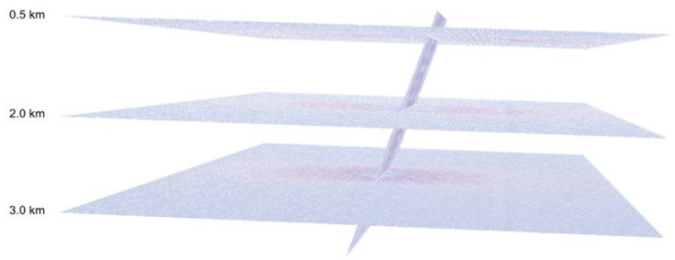

Figure 1. Fault model geometry in sideview. The topmost observation layer is located at 0.5 km-depth beneath the surface; the middle observation layer is located at 2.0 km-depth; and the bottommost layer is located at 3.0 km-depth. The fault plane dips at 70 degrees from the horizontal.

the same manner as the FP models: first 10 m of slip, then 50 m, and finally 200 m (Fig. 2).

DATA AND RESULTS

Damage zone distributions

In every scenario, the locations of MCSS and E1 maximums and minimums are nearly identical, indicating that stress and strain vary in an identical manner within a given model. Near the fault center, the predicted variable values are greater than for the same variable at the fault tips. I also used the same set of fault displacements (10, 50, and 200 meters) for all models. In all models, greater fault displacement is associated with proportionally higher predictions of MCSS, E1, and dilation values. However, the location and width of elevated stress and strain values (i.e. damage zones) for each model remains consistent, regardless of increasing vertical displacement. Fracture intensity is also greatest where stress and strain values are highest, and decreases away from damage zones (Fig. 3).

Depth

The top observation surface in each model predicts greater areas of elevated E1 and MCSS values (i.e. damage zones) within the hanging wall, relative to the footwall. But, as depth increases, the location of major damage zones shifts towards the fault plane, such that they occur in the footwall at depth. The numerical values of MCSS, E1, and dilation predicted by the models also change between observation surfaces; within the same model, the middle observation surface (2 km depth) predicts the highest values, with the bottom layer displaying slightly lower values, and the top observation surface demonstrating the lowest (Fig. 4).

Fault growth models (FP vs. CL)

For the different fault propagation models, the relative location of MCSS, E1, and dilation maximums and minimums for each observation surface remains consistent, with the highest values observed near the fault center, and decreasing values associated with the fault tips. However, this pattern is shortened proportionally to the fault plane in the start and middle stages of the FP model. Numerically, the fault propagation models at every stage generate greater predicted E1, MCSS, and dilation values than for the constant length models experiencing the same vertical displacement, in the same material, and measured at the same depth (Fig. 5).

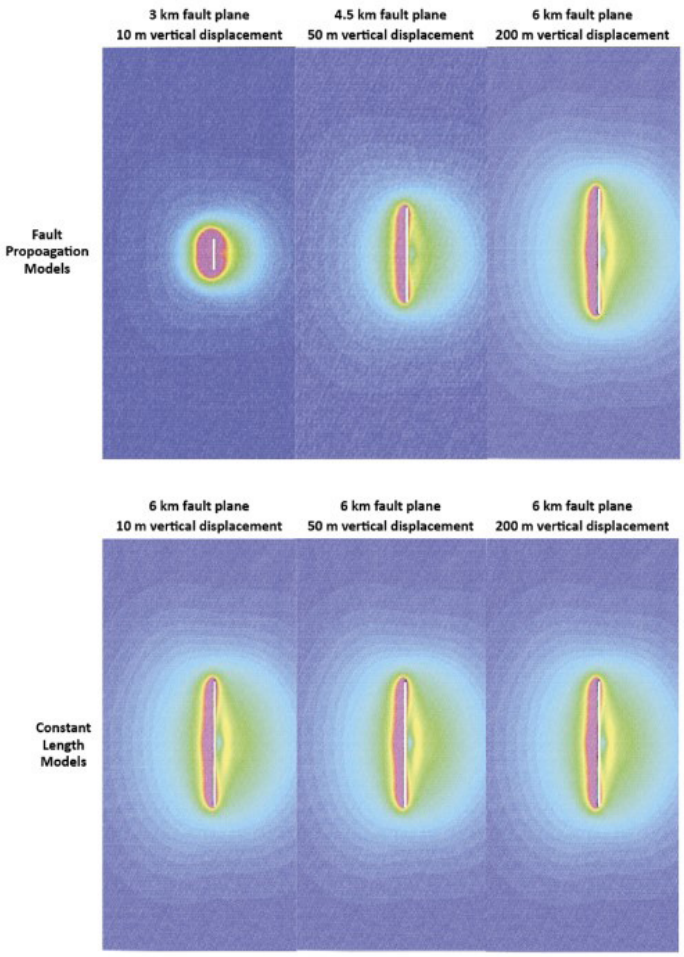

Figure 2. Fault Propagation and Constant Length fault growth models. Constructed models simulating the Fault Propagation (top) and Constant Length (bottom) theories of fault growth. Models are shown from the top, with fault lengths represented by white lines. The hanging wall lies to the left of each fault plane, and the footwall lies on the right. Fault models are overlain by MCSS predictions for a 6 km fault plane (shown at 0.5km of depth) experiencing 200 m of displacement, approximating the CL End model. Warmer values indicate greater MCSS values.

Pore fluid pressure

The location and volumetric extent of damage zones between models with different pore fluid pressures remain consistent. However, the specific values predicted for MCSS, E1, and dilation vary such that models with a set PFP value of 0 MPa predict lower MCSS and E1 values at a given point, relative to an equivalent model with realistic pore fluid pressures.

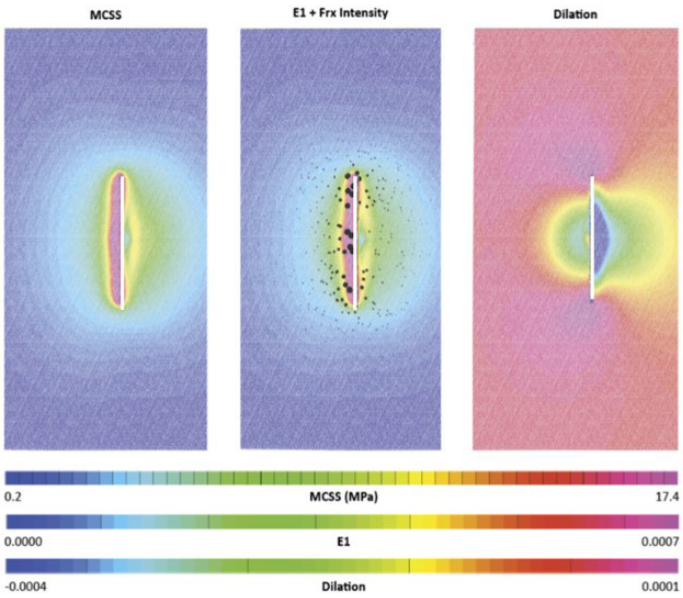

Figure 3. Distribution of damage zones. Predicted MCSS (left), E1 (middle), and dilation (right) values for the 0.5 km depth surface of a model experiencing 200 meters of vertical displacement along a 6 km fault plane. This model represents the Constant Length model with realistic pore fluid pressures included. Warmer colors represent higher values; cooler colors represent lower values. Fracture intensity is also depicted on the E1 surface, with larger black dots representing greater fracture intensity at a given point.

For example, the maximum MCSS value predicted in the CL End model with 0 MPa of PFP is just over 600 MPA; in the same model but with realistic PFP values, the maximum MCSS value predicted is about 800 MPa.

DISCUSSION

Damage zone distributions

In all models, the greatest values of stress and strain occur adjacent to the fault plane and decrease with distance. This trend is also well-documented in field studies, with the frequency of fault-related deformation greatest near the fault (e.g., Choi, 2016; Childs et al., 2009). The width of damage zones also appears consistent between models, even as displacement increases, mirroring a consistent damage zone model proposed by Ferrill and Morris (2001). However, previous field studies, as summarized by Houwers et. al. (2015), suggest increasing fault displacement corresponds to widening damage zones. Because the FRM module does not account for pre-existing weaknesses and thus negates the potential deformational influence of early fracturing, I cannot offer insight into which of these patterns is more realistic, though this represents a potential area for future research.

Furthermore, the higher predicted stress and strain values present away from the fault plane in the hanging wall of the 0.5 km observation surface of the models, relative to the footwall, suggest that damage zones form asymmetrically across normal fault planes. Such asymmetry has been documented in a field study of the same lithology (Navajo sandstone), with a narrower damage zone in the footwall (70 m) of the normal fault versus the hanging wall (210 m) (Berg and Skar, 2005).

Change in damage zone distributions with depth

Every model demonstrates damage zone asymmetry, though the direction varies with depth. I have not found studies that provide a satisfying cause for this switch in damage zone location with depth. However, fault slip tapering and related propagation direction may play a role. Fault slip tapering refers to displacement which is greatest at the fault center and decreases to 0 at fault tips, as observed in field studies. This fault slip distribution is represented in my modeling. Because displacement accumulates, the fault plane above the centroid represents an area on the fault plane that experiences upward propagation of accumulating displacement, and the fault plane below represents an area that experiences downward propagation of displacement. The fault dips at an angle and strain-related fracturing propagates in an orientation that is more energetically favorable, especially based on propagation direction (e.g., Sharon and Fineberg, 1996; Zhou et al., 2018; Fineberg and Bouchbinder, 2015; Surpless and McKeighan, 2022); thus, propagation direction may explain damage zone asymmetry.

Fault growth models: fault propagation vs. constant length

By comparing the damage zone extents between my Fault Propagation and Constant Length models, it is clear that damage zones tend to follow the same distribution of high stress and strain around the fault plane, regardless of propagation model or stage. However, the sizes of these damage zones

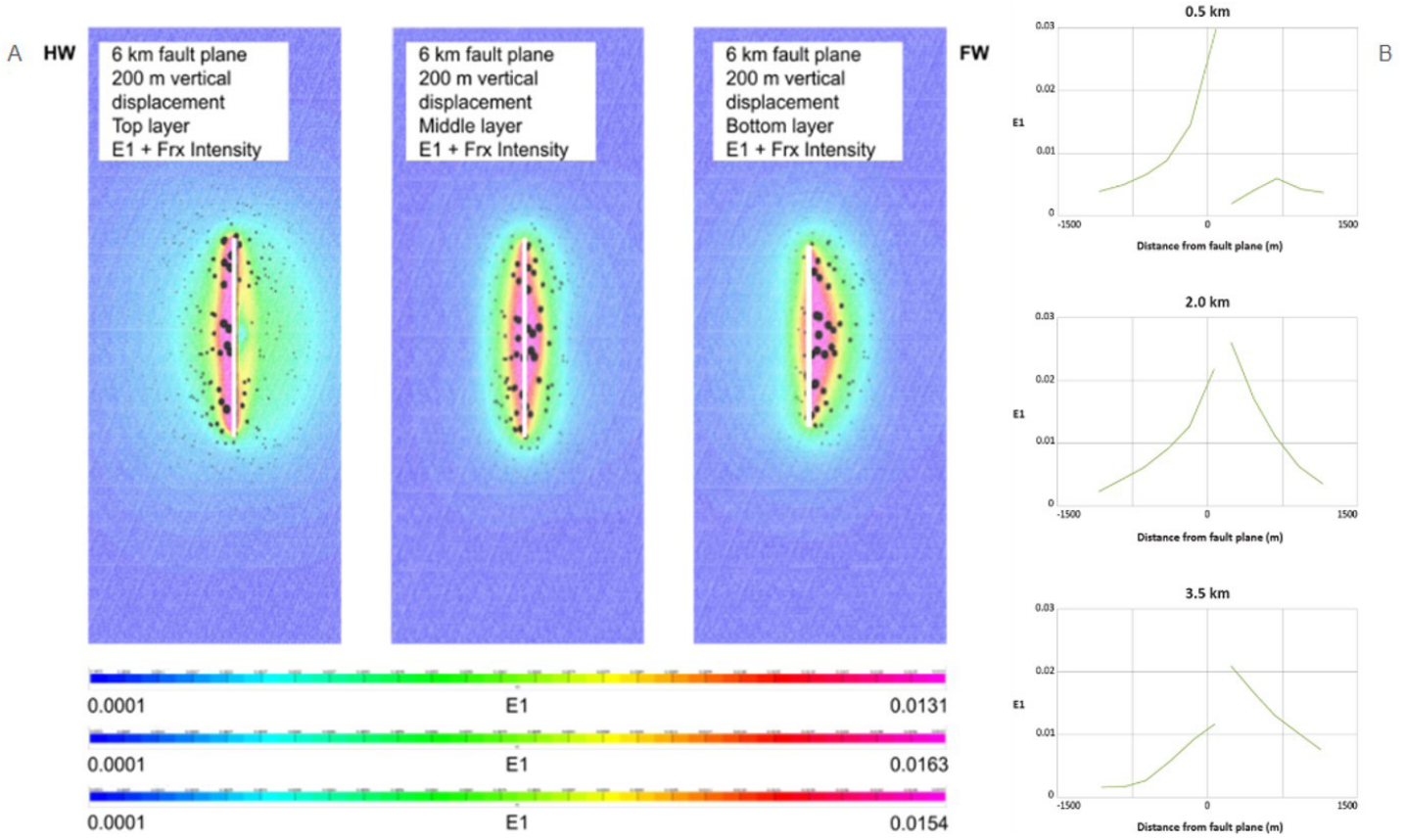

Figure 4. A) Damage zone distribution with depth. Predicted E1 values and fracture intensities for the 0.5 km-depth surface (left), 2 km-depth surface (middle), and 3.5 km-depth surface (right) of a 6 km fault plane experiencing 200 m of vertical displacement. These models represent 3 different depths of the CL End stage of the Constant Length growth model. Warmer colors represent higher values; cooler colors represent lower values. Fracture intensity is also depicted on the E1 surface, with larger black dots representing greater fracture intensity at a given point. B) Graphical representations of E1 values at 0.5 km (top), 2.0 km (middle), and 3.5 km (bottom) depths around a 6 km fault plane experiencing 200 m of vertical displacement. These models represent 3 different depths of the CL End stage of the Constant Length growth model. As depth increases, elevated E1 values shift from the hanging wall side of the graph (0.5 km depth) to the footwall side of the graph (3.0 km depth).

vary with fault propagation model stage such that the shorter fault planes of early-stage FP models generated proportionally shorter damage zones in the fault-parallel direction. Still, both the FP model set and the CL model set concluded with a 6 km fault plane experiencing 200 m of vertical depth, and the associated stress and strain variable predictions for these final stages of each model set produced essentially identical damage zone distributions. Such a discrepancy in damage zone area between early-stage FP and CL models indicates that damage zones would form differently based on the relationship between fault propagation and displacement accumulation; however, fault zones with the same fault length and amount of displacement may ultimately have similar damage zone distributions regardless of growth history.

Influence of pore fluid pressure

My models also indicate that systems with realistic pore fluid pressures (PFPs) record higher MCSS and E1 values than systems with PFP values of 0. When considering the Mohr Coulomb failure envelope, failure in material occurs if the shear and normal stress values are such that the Mohr circle intersects the failure envelope. Higher pore fluid pressure shifts the Mohr circle towards the left, meaning that failure is far more likely to occur. The elevated strain values observed in models with realistic PFP values, relative to in models with no PFP, thus likely reflect the leftwards shift towards failure and a potential for increased permeability.

Fracturing intensity and orientation

Understanding fracture intensity and orientation

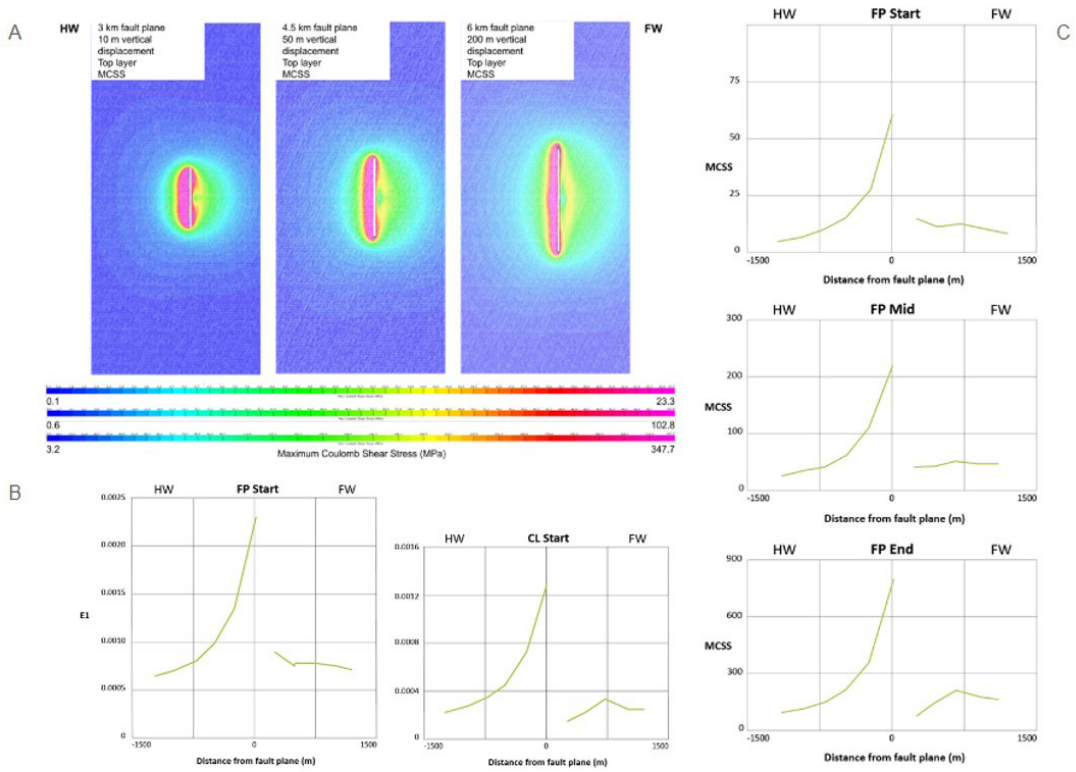

Figure 4. A) Fault propagation (FP) model of fault growth. Predicted MCSS for the 0.5 km depth surface of a 3 km fault plane experiencing 10 m of vertical displacement, representing the FP start model (left); a 4.5 km fault plane experiencing 50 m of vertical displacement, representing the FP Mid model (middle); and a 6 km fault plane experiencing 200 m of vertical displacement, representing the FP End stage of the Fault Propagation model of fault growth. Models include realistic pore fluid pressures. Warmer colors represent higher values; cooler colors represent lower values. B) Graphical representations of E1 predicted for a 3 km fault plane experiencing 10 m of vertical displacement, representing the FP Start stage of the Fault Propagation model (left) and a 6 km fault plane experiencing 10 m of vertical displacement, representing the CL Start stage of the Constant Length fault growth model. For the same stage (starting vs. ending) in the FP fault growth model (left) and the CL fault growth model (right), predicted MCSS and E1 values are higher in the FP models compared to the CL models. C) Graphical representations of MCSS values for the FP model shown in A. As fault propagation within the Fault Propagation conceptual model of fault growth continues, predicted MCSS values increase.

predictions is especially important for assessment of geothermal potential because increases in permeability created by fracturing and dilation create the primary pathways for circulating geothermal fluids in fault systems. My modeling results indicate that fracture intensities are greatest in regions of elevated stress and strain, meaning that the locations of high intensity fracturing in each model are subject to the same trends observed in damage zone locations.

CONCLUSION

Implications for geothermal energy

Based on my model results and published field studies, the location and nature of damage zone development around a normal fault system can vary, depending on factors like 1) amount of vertical displacement experienced by the fault, 2) stage of fault propagation; 3) pore fluid pressure; and 4) depth (in relation to the slip-tapering centroid). The high fracture intensities and dilation values (and thus likely high permeability) observed in the damage zones of my models provide insights into damage zone development that can be used to better understand geothermal energy potential in normal fault zones and for constraining potential targets for future field-based geothermal exploration. Given that geothermal energy is one of the most promising renewable energy resources of the 21st century, with the potential to generate 2-4 times as much electricity as wind or solar energy at the same installed capacity, finding ways to minimize the cost of geothermal exploration will be crucial for promoting green energy and developing resilient electricity through resource diversification (U.S. Department of Energy, 2019). 3D modeling, which can be done in advance of expensive field studies, represents a potential method for better identifying damage zones that can support utility-scale geothermal energy

production.

ACKNOWLEDGMENTS

This material is based upon work supported by the Keck Geology Consortium and the National Science Foundation under Grant No. 2050697.

REFERENCES

Berg, S.S., and Skar, T., 2005, Controls on damage zone asymmetry of a normal fault zone: outcrop analyses of a segment of the Moab fault, SE Utah: Journal of Structural Geology, v. 27, p. 803-1822.

Boden, D.R., 2017, Geologic Fundamentals of Geothermal Energy: Boca Raton, Florida, CRC Press, 399 p.

Childs, C., Manzocchi, T., Walsh, J.J., Bonson, C.G., Nicol, A., Schoepfer, M.P.J., 2009, A geometric model of fault zone and fault rock thickness variations, Journal of Structural Geology, v. 31, p. 117 - 127.

Choi, J.H., Edwards, P., Ko K., and Kim, Y.S., 2016, Definition and classification of fault damage zones: A review and a new methodological approach: Earth-Science Reviews, v. 152, p. 70 – 87.

Cooke, M., unpublished, Numerical Methods – Boundary Element Modeling, 3p.

Cowie, P.A., and Shipton, Z.K., 1998, Fault Tip Displacement Gradients and Process Zone Dimensions, Journal of Structural Geology, v. 20, p. 983 - 997.

Crider, J., and Pollard, D., 1998, Fault linkage: Three-dimensional mechanical interaction between echelon normal faults, Journal of Geophysical Research, v. 103, p. 24.373 - 24.391.

Faulds, J., and Hinz, N., 2015, Favorable Tectonic and Structural Settings of Geothermal Systems in the Great Basin Region, Western USA: Proxies for Discovering Blind Geothermal Systems, in Proceedings, World Geothermal Congress, Melbourne: Australia, Nevada Bureau of Mines and Geology (https://www.osti.gov/servlets/purl/1724082).

Ferrill, D.A., and Morris, A.P., 2001, Displacement gradient and deformation in normal fault systems, Journal of Structural Geology, v.23, p. 619 – 638.

Fineberg, J., and Bouchbinder, E., 2015, Recent developments in dynamic fracture: Some perspectives, International Journal of Fracture, v.196, 33 – 57.

Fossen, H., and Rotevatn, A., 2015, Fault linkage and relay structures in extensional settings- A review, Earth Science Reviews.

Fossen, H., 2016, Structural Geology: 2nd edition, Cambridge: Cambridge University Press.

Houwers, M.E., Heijnen, L.J., Becker, A., Rijkers, R., 2015, A Workflow for the Estimation of Fault Zone Permeability for Geothermal Production: A General Model Applied on the Roer Valley Graben in the Netherlands, in Proceedings, World Geothermal Congress, Melbourne: Australia.

Kim, Y.S., Peacock, D., Sanderson, D, 2004., Fault damage zones: Journal of Structural Geology v. 26. P. 503 - 517. DOI: 10.1016/j.jsg.2003.08.002.

Kim, Y.S., and Sanderson, D., 2005, The relationship between displacement and length of faults: A review, Earth Science Reviews, v. 68, p. 317 – 334.

Liao, Z., Hu, L., Huang, X., Carpenter, B.M., Marfurt, K.J., Vasileva, S., and Zhou, Y., 2020, Characterizing damage zones of normal faults using seismic variance in the Wangxuzhuang oilfield, China: Interpretations v. 8, p. 1- 24.

Micale, V., Oliver, P., and Messent, F., 2014, The Role of Public Finance in Deploying Geothermal: Background Paper, in San Giorgio Group Report, Climate Policy Initiative, p. 1 - 15.

Nicol, A., Childs, C., Walsh, J.J., Manzocchi, T., Schopfer, M.P.J., 2017, Interactions and growth of faults in an outcrop-scale system, Geological Society of London Special Publications, v. 439, p. 23 – 39.

Petex, 2020, Move 2020 Tutorial 33: Fault Response Modeling.

Rotevatn, A., Jackson, C.A.L., Tvedt, A.B.M, Bell, R.E., Blaekkan, I., 2019, How do normal faults grow? Journal of Structural Geology, v. 125, p. 174 – 184.

Savage, H.M., Brodsky, E.E., 2011, Collateral damage: Evolution with displacement of fracture distribution and secondary fault strands in fault damage zones, v. 116, p. 1 – 14.

Schultz, R., 2010, Porosity and Grain Size Controls

on Compaction Band Formation in Jurassic Navajo Sandstone: American Geological Union geophysical Research Letters v. 37, 22.
Sharon, E., Fineberg, E., 1996, Microbranching instability and the dynamic fracture of brittle materials: Physics Reviews, v. B54, p. 7128–7139.
Shervais, J. et al., 2024, Geothermal play fairway analysis, part 1: Example from the Snake River Plain, Idaho, v. 117, p. 1 – 18.
Surpless, B.E., and McKeighan, C., 2022, The role of dynamic fracture branching in the evolution of fracture networks: an outcrop study of the Jurassic Navajo Sandstone, southern Utah: Journal of Structural Geology, v. 161. DOI: 10.1016/j.jsg.2022.104664.
U.S. Department of Energy, 2019, Geovision: Harnessing the Heat Beneath our Feet: https://www.energy.gov/sites/prod/files/2019/06/f63/GeoVision-full-report-opt.pdf (accessed September 2023)
Zhou, S., Zhuang, X., Zhu, H., Rabczuk, T., 2018, Phase field modeling of crack propagation -Branching Coalescence Rocks: Theoretical Applications of Fracture Mechanics, v. 96, p. 174–192.